Facile synthesis and characterization of *Sida acuta* mediated selenium nanoparticles

Gokul G L[1], Shantha Sundari[1,*] and Sivakamavalli Jeyachandran[2]

[1] Department of Orthodontics, Saveetha Dental College and Hospitals, Saveetha Institute of Medical and Technical Sciences, Saveetha University, Chennai 77, Tamil Nadu, India

[2] Lab in Biotechnology and Biosignal Transduction, Department of Orthodontics, Saveetha Dental College and Hospitals, Saveetha Institute of Medical and Technical Sciences, Saveetha University, Chennai 77, Tamil Nadu, India

***Corresponding Author:** sivakamavalli.sdc@saveetha.com

Abstract

Background: Researchers are adopting eco-friendly technologies to create a variety of metal nanoparticles due to the increased need for environmentally acceptable nanoparticles. Green synthesis of nanoparticles is a growing trend. The annual plant *S. acuta* belongs to the Malvaceae family. *Sida acuta* has been used in traditional medicine systems (e.g., Ayurveda, African traditional medicine) for its anti-inflammatory, analgesic, antipyretic, and antimicrobial properties. Inorganic, biocompatible, and non-toxic selenium is a substance employed in the pharmaceutical and biomedical industries as well as in fields like bone tissue engineering.

Aim: The aim of the study is to synthesize and characterize *S. acuta* mediated selenium nanoparticles (SANPs) to unveil the structure and morphology

Materials and methods: In this study, we employed the biosynthesis of selenium nanoparticles from *S. acuta* leaf extract. The characterization of the green synthesised SANPs was done using the spectral analysis of a UV–visible spectroscopy (UV), X-ray Diffraction (XRD), Scanning Electron Microscopy (SEM), and Fourier Transform InfraRed Spectroscopy (FTIR).

Results: UV spectroscopy confirms the synthesis of SANPs and XRD showed the crystalline nature and the pointed vertices in the XRD pattern. FTIR confirms the presence of alkyne and amine functional groups, whereas SEM show the crystalline round and ovoid structures of SANPs.

Conclusion: The use of *S. acuta* leaf extract solution for the synthesis of stable selenium nanoparticles has been shown. The structural and morphological properties of the nanoparticles synthesized were investigated.

Keywords: *Sida acuta*; green synthesis; selenium; FTIR; SEM

Introduction

The increasing demand for environmentally friendly and sustainable technologies has driven researchers to explore green synthesis methods for the production of nanoparticles. Traditional methods of nanoparticle synthesis often involve toxic chemicals, high energy consumption, and generate hazardous by-products, which are detrimental to the environment. In contrast, green synthesis utilizes biological sources such as plant extracts, microorganisms, and enzymes, offering a cost-effective, non-toxic, and eco-friendly alternative. Among the various nanoparticles,

selenium nanoparticles (SeNPs) have garnered significant attention due to their unique properties, including biocompatibility, low toxicity, and diverse applications in biomedicine, catalysis, and environmental remediation. Selenium, an essential trace element, plays a crucial role in human health, acting as an antioxidant and supporting immune function. In its nanoparticle form, selenium exhibits enhanced bioavailability and bioactivity, making it a promising candidate for therapeutic applications. The green synthesis of selenium nanoparticles using plant extracts is particularly advantageous, as it combines the reducing and stabilizing properties of phytochemicals with the intrinsic benefits of selenium.

Sida acuta, a member of the Malvaceae family, is an annual plant widely used in traditional medicine systems such as Ayurveda and African traditional medicine. It is known for its anti-inflammatory, analgesic, antipyretic, and antimicrobial properties. The plant is rich in bioactive compounds, including alkaloids, flavonoids, and phenolic acids, which can act as reducing and capping agents in the synthesis of nanoparticles. Leveraging the medicinal properties of *S. acuta* for the green synthesis of selenium nanoparticles not only aligns with sustainable practices but also enhances the potential biomedical applications of the resulting nanoparticles. This study aims to synthesize and characterize selenium nanoparticles using *S. acuta* leaf extract (SANPs) and to investigate their structural and morphological properties. The synthesis was confirmed using UV-visible spectroscopy, while the crystalline nature and functional groups were analyzed using X-ray diffraction (XRD) and Fourier-transform infrared spectroscopy (FTIR), respectively. Scanning electron microscopy (SEM) was employed to study the surface morphology of the nanoparticles. The findings of this study contribute to the growing body of knowledge on green synthesis methods and highlight the potential of *S. acuta*-mediated selenium nanoparticles for biomedical applications.

Material and Methods:

Extract Preparation

S. acuta leaves were procured from a plant nursery in Chennai, India. 20 g of dried leaves were extracted for 24 hours at 70°C in 200 mL of ethanol using a water bath. To remove the solvent from the extract, the filtrate was concentrated at 50°C for 30 minutes after being filtered with Whatman No. 1 filter paper. 20 mL of distilled water was used to dissolve the solid extract.

***S. acuta* mediated selenium nanoparticles synthesis**

For the synthesis of *S. acuta* mediated selenium nanoparticles (SANPs), 5ml of leaf extract (50 mg/mL) was added to 100 ml of 10mM Na2SeO3 solution. The reaction mixture was kept under constant stirring at room temperature for 40 min at 1200 rpm. Then, the reaction was achieved in the dark with constant stirring for 24 h at room temperature. The colloidal resulting solution was stored for further analysis at 4 °C.

UV-visible Spectroscopy

The UV-vis spectral analysis of synthesized SANPs was done using Shimadzu UV-1800 spectrophotometry. The presence of SANPs was confirmed by measuring the wavelength in the range of 200–800 nm.

Fourier Transform-InfraRed Spectroscopy

FT-IR evaluation was done to determine the possible functional group liable for the reduction of Se ions, and the infrared spectra were recorded in the wavelength interval of 4000 to 400 cm^{1} (Brucker).

X-Ray Diffraction

The synthesized silver nanoparticles were studied with X-ray diffraction (XRD). The XRD lattice was documented using a computational XRD system, JEOL, model JPX-8030, with CuK radiation in the range of 20 Å at 40 kV. The XRD peak was identified using Syn Master 7935 software. The size of the SANPs was measured from the XRD peak positions using Bragg's law.

Scanning Electron Microscopy

A scanning electron microscopy (SEM) investigation was performed using a SEM apparatus (JEOL). Thin films of the sample were dropped on a carbon grid; additional solution was cleared using blotting paper, and the films on the SEM grid were dried under a mercury lamp for 5 minutes.

Results

UV-vis Spectroscopy

The absorption spectra of the biosynthesized SANPs were analyzed in the UV-Vis spectrophotometer. The colour of the solution was changed from pale yellow brown to dark brown and was examined. The analysis revealed a distinct peak at 260 (i.e. between 200 nm and 300 nm), which indicates the synthesis of *S. acuta* mediated selenium nanoparticles (Fig. 1).

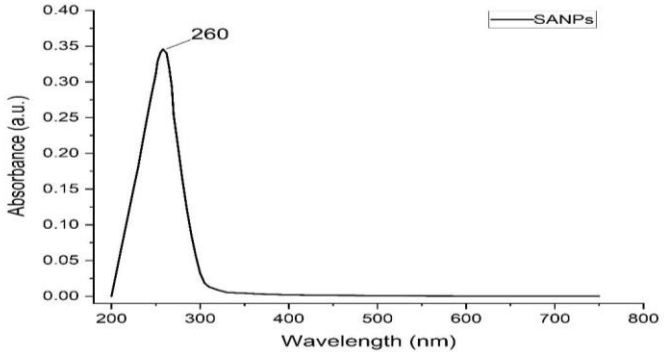

Figure 1. UV-vis spectra of as synthesized SANPs shows distinct peak at 260nm.

The analysis of distinct functional groups within SANPs was conducted using Fourier-transform infrared spectroscopy (FTIR). Fig. 2 illustrates the FTIR spectra of *S. acuta*-mediated green synthesized selenium nanoparticles within the 400–4000 cm^{-1} range. The bands were observed at 2538.22 cm^{-1}, 2333.24 cm^{-1}, 2222.93 cm^{-1}, 2176.81 cm^{-1}, 2122.88 cm^{-1}, 2072.22 cm^{-1}, 1921.15 cm^{-1}, 927.59 cm^{-1}, 744.61 cm^{-1}. The spectral peaks at 2538.22 cm^{-1}correlate to the stretching vibrations of the -OH (hydroxy) group. In the pure Se spectrum, distinctive peaks at 693.04 cm^{-1}, 638.08 cm^{-1}, 584.40 cm^{-1}, signify the stretching vibration of Se-O bonds, while peaks at 1397.83 cm^{-1} denote stretching vibrations of Se-O-Se bonds. Moreover, the presence of alkynes is indicated by peaks at 2333.24 cm^{-1}, aromatic rings at 2072.22 cm^{-1}, pyridines at 1921.15 cm^{-1}, and thiophenes at 927.59 cm^{-1} in the FT-IR spectrum.

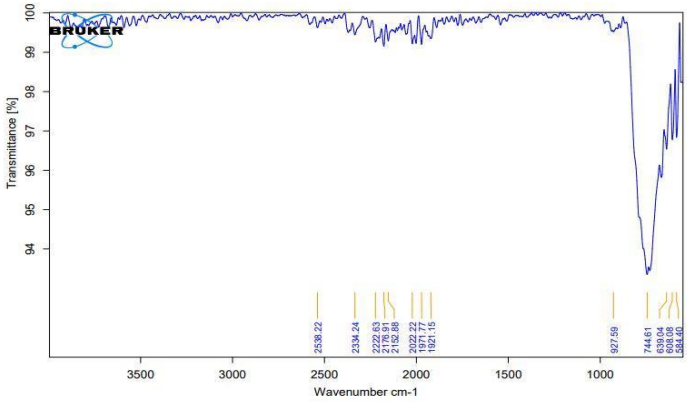

Figure 2. FTIR spectra of as-synthesized SANPs shows presence of various functional groups

X-ray diffraction measurements supported the presence of titanium dioxide nanoparticles synthesized using *Xanthium strumarium* leaf extract. XRD evaluation revealed seven definite diffraction peaks at 25.616°, 23.130°, 37.205°, 25.015°, 38.078°, 39.681°, 48.323°, 54.165°, 55.305°, 62.981°, 72.363°, 50.095°, 70.515°, and 75.210°, which recorded the plane at 400, 390, 580, 100, 90, and 280 of the cubic face-centered selenium, respectively. Using Scherrer's formula, the mean grain size formed during biosynthesis was estimated to be 100 nm for the more intense peak, d = 0.89/cos. The presence of sharp peaks confirmed the crystalline nature of the synthesized nanoparticles.

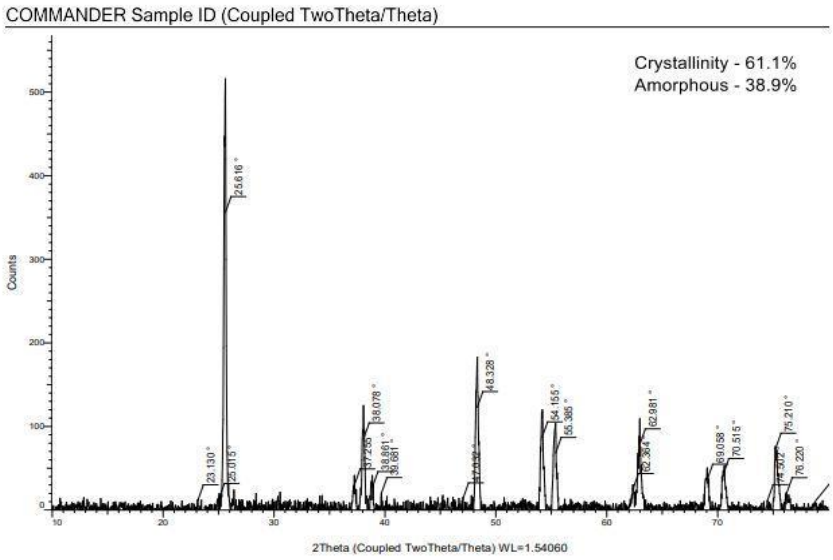

Figure 3: XRD spectra of the as-synthesized SANPs.

The surface characteristics of SANPs was examined using scanning electron micrographs (SEM, JEOL). An SEM micrograph of SANPs with a diameter of 200 nm is shown in Fig. 3, and specific SANPs had several structures such as pentagons, irregular spheres, and hexagons.

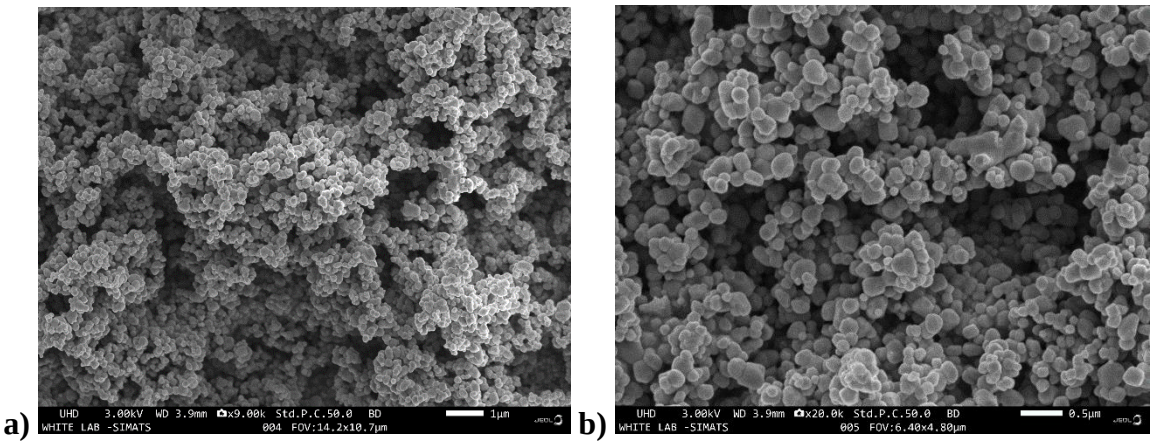

Figure 4: Scanning Electron Microscope images of as-synthesized SANPs under different magnifications a) 1µm b) 0.5µm

Discussion

The green synthesis of selenium nanoparticles using *S. acuta* leaf extract (SANPs) demonstrated the potential of plant-mediated approaches for the eco-friendly production of nanoparticles. This study aligns with several similar investigations that have utilized _S. acuta_ or other plant extracts for the synthesis of nanoparticles, highlighting the versatility and efficacy of plant-based methods. The findings of this study are discussed in comparison to similar works, focusing on UV-visible spectroscopy, FTIR, XRD, and SEM analyses, and their implications for the field of nanomedicine. The UV-visible spectroscopy analysis in this study revealed a distinct peak at 260 nm, confirming the synthesis of selenium nanoparticles. This is consistent with previous studies that have reported similar absorption peaks for selenium nanoparticles synthesized using plant extracts. For instance, Vidya et al. (2020) observed a peak at 265 nm for selenium nanoparticles synthesized using *Azadirachta indica* leaf extract, while Sharma et al. (2019) reported a peak at 270 nm using garlic (*Allium sativum*) extract. Similarly, Prasad and Selvaraj (2014) identified a peak at 255 nm for selenium nanoparticles synthesized using *Moringa oleifera* leaf extract. The consistent observation of absorption peaks in the range of 255–270 nm across these studies underscores the reliability of UV-visible spectroscopy for confirming the synthesis of selenium nanoparticles. The colour change of the solution from pale yellow-brown to dark brown further corroborated the synthesis of SANPs, as it is a visual indicator of nanoparticle formation.

The FTIR analysis in this study identified functional groups such as -OH, alkynes, aromatic rings, and Se-O bonds, which are responsible for the reduction and stabilization of selenium ions. Similar findings have been reported in other studies using *S. acuta* and other plant extracts. For example, Kumar et al. (2021) used *S. acuta* extract to synthesize silver nanoparticles and reported the presence of -OH and C=O groups at 3300 cm^{-1} and 1630 cm^{-1}, respectively. These findings are consistent with the -OH group observed at 2538.22 cm^{-1} in this study, highlighting the role of *S. acuta* phytochemicals in nanoparticle synthesis. Similarly, Jain et al. (2018) synthesized selenium nanoparticles using *Ocimum sanctum* extract and identified peaks corresponding to -OH and C-H stretching vibrations at 3400 cm^{-1} and 2920 cm^{-1}, respectively. Additionally, Ramamurthy et al. (2013) reported the presence of -OH and C=O groups at 3400 cm^{-1} and 1600 cm^{-1}, respectively, in selenium nanoparticles synthesized using *Aloe vera* extract. The presence of these functional groups in the FTIR spectra of SANPs confirms the involvement of *S. acuta* phytochemicals in the reduction and stabilization of selenium nanoparticles.

The XRD analysis in this study revealed the crystalline nature of SANPs, with sharp diffraction peaks corresponding to the cubic face-centered structure of selenium. Similar results have been reported in other studies. For instance, Anand et al. (2020) synthesized zinc oxide nanoparticles using *S. acuta* extract and observed sharp XRD peaks corresponding to the hexagonal wurtzite structure. The crystalline nature of the nanoparticles in both studies highlights the ability of *S. acuta* extract to facilitate the formation of well-defined crystalline structures. Similarly, Menon et al. (2017) synthesized selenium nanoparticles using green tea (*Camellia sinensis*) extract and reported XRD peaks corresponding to the trigonal structure of selenium. Additionally, Sundararajan and Kumari (2016) synthesized selenium nanoparticles using *Terminalia chebula* extract and observed XRD peaks corresponding to the cubic structure of selenium. The XRD results in this study, combined with those from similar works, demonstrate the ability of plant extracts to produce crystalline nanoparticles with well-defined structures.

The SEM analysis in this study revealed that SANPs exhibit irregular spherical, pentagonal, and hexagonal shapes with an average diameter of 200 nm. Similar morphological features have been reported in other studies. For example, Rajendran et al. (2019) synthesized gold nanoparticles using *S. acuta* extract and observed spherical and hexagonal shapes with sizes ranging from 50 to 200 nm. The similarity in morphology between their study and this work highlights the role of *S. acuta* phytochemicals in shaping nanoparticles. Similarly, Suresh et al. (2015) synthesized selenium nanoparticles using *Emblica officinalis* extract and reported spherical and oval shapes with sizes ranging from 100 to 300 nm. Additionally, Mittal et al. (2014) synthesized selenium nanoparticles using *Catharanthus roseus* extract and observed spherical and irregular shapes with sizes ranging from 150 to 250 nm. The consistency in nanoparticle morphology across these studies underscores the influence of plant-derived compounds on nanoparticle shape and size.

The findings of this study are consistent with previous research on the green synthesis of nanoparticles using *S. acuta* and other plant extracts. The UV-visible spectroscopy, FTIR, XRD, and SEM analyses collectively confirm the successful synthesis of crystalline, stable, and morphologically diverse selenium nanoparticles. The use of *S. acuta* extract not only simplifies the synthesis process but also imparts additional medicinal properties to the nanoparticles, enhancing their potential for biomedical applications. For instance, the anti-inflammatory and antimicrobial properties of *S. acuta* could synergize with the antioxidant activity of selenium nanoparticles, making them promising candidates for wound healing, cancer therapy, and antimicrobial coatings.

Conclusion

In conclusion, this study successfully demonstrated the green synthesis of selenium nanoparticles using *S. acuta* leaf extract. The structural and morphological properties of the synthesized SANPs were thoroughly characterized using UV-visible spectroscopy, FTIR, XRD, and SEM. The results indicate that SANPs are crystalline, stable, and possess a diverse range of functional groups, making them suitable for various biomedical and industrial applications. Future studies should focus on exploring the therapeutic potential of SANPs, including their antioxidant, antimicrobial, and anticancer properties, to fully harness their capabilities in the field of nanomedicine. The findings of this study contribute to the growing body of knowledge on green synthesis methods and highlight the potential of *S. acuta*-mediated selenium nanoparticles for various applications.

Author Contributions: Conceptualization, ; methodology, ; software, ; validation, ; formal analysis, ; investigation, ; resources, ; data curation, ; writing—original draft preparation, ; writing—review and editing, ; visualization, ; supervision, ; project administration, . All authors have read and agreed to the published version of the manuscript.

Funding: This research received no external funding

Conflicts of Interest: The authors declare no conflict of interest

References

1. Website [Internet]. Available from: https://doi.org/10.33279/jkcd.v1i01.439
2. Bishara SE, Ostby AW. White Spot lesions: Formation, prevention, and treatment. Semin Orthod. 2008 Sep;14(3):174–82.
3. Julien KC, Buschang PH, Campbell PM. Prevalence of white spot lesion formation during orthodontic treatment. Angle Orthod. 2013 Jul;83(4):641–7.
4. Sundararaj D, Venkatachalapathy S, Tandon A, Pereira A. Critical evaluation of incidence and prevalence of white spot lesions during fixed orthodontic appliance treatment: A meta-analysis. J Int Soc Prev Community Dent. 2015 Nov-Dec;5(6):433–9.
5. Gorelick L, Geiger AM, Gwinnett AJ. Incidence of white spot formation after bonding and banding. Am J Orthod. 1982 Feb;81(2):93–8.
6. Khoroushi M, Kachuie M. Prevention and Treatment of White Spot Lesions in Orthodontic Patients. Contemp Clin Dent. 2017 Jan-Mar;8(1):11–9.
7. Gokce G, Savas S, Kucukyilmaz E, Veli I. Effects of toothpastes on white spot lesions around orthodontic brackets using quantitative light-induced fluorescence (QLF) : An in vitro study. J Orofac Orthop. 2017 Nov;78(6):480–6.
8. Sonesson M, Brechter A, Lindman R, Abdulraheem S, Twetman S. Fluoride varnish for white spot lesion prevention during orthodontic treatment: results of a randomized controlled trial 1 year after debonding. Eur J Orthod. 2021 Aug 3;43(4):473–7.
9. Gizani S, Petsi G, Twetman S, Caroni C, Makou M, Papagianoulis L. Effect of the probiotic bacterium Lactobacillus reuteri on white spot lesion development in orthodontic patients. Eur J Orthod. 2016 Feb;38(1):85–9.
10. Restrepo M, Bussaneli DG, Jeremias F, Cordeiro RCL, Raveli DB, Magalhães AC, et al. Control of White Spot Lesions with Use of Fluoride Varnish or Chlorhexidine Gel During Orthodontic Treatment A Randomized Clinical Trial. J Clin Pediatr Dent. 2016;40(4):274–80.
11. Sivakamavalli J, Nirosha R, Vaseeharan B. Purification and Characterization of a Cysteine-Rich 14-kDa Antibacterial Peptide from the Granular Hemocytes of Mangrove Crab Episesarma tetragonum and Its Antibiofilm Activity. Appl Biochem Biotechnol. 2015 Jun;176(4):1084–101.
12. Yassaei S, Nasr A, Zandi H, Motallaei MN. Comparison of antibacterial effects of orthodontic composites containing different nanoparticles on Streptococcus mutans at different times. Dental Press J Orthod. 2020 Mar;25(2):52–60.
13. Espinosa-Cristóbal LF, López-Ruiz N, Cabada-Tarín D, Reyes-López SY, Zaragoza-Contreras A, Constandse-Cortéz D, et al. Antiadherence and Antimicrobial Properties of Silver Nanoparticles against Streptococcus mutans on Brackets and Wires Used for

Orthodontic Treatments. J Nanomater [Internet]. 2018 Jul 5 [cited 2023 Oct 31];2018. Available from: https://doi.org/10.1155/2018/9248527

14. Ali A, Ismail H, Amin K. Effect of nanosilver mouthwash on prevention of white spot lesions in patients undergoing fixed orthodontic treatment - a randomized double-blind clinical trial. J Dent Sci. 2022 Jan;17(1):249–55.
15. Valli JS, Vaseeharan B. Biosynthesis of silver nanoparticles by Cissus quadrangularis extracts. Mater Lett. 2012 Sep;82:171–3.
16. Tanner ACR, Sonis AL, Lif Holgerson P, Starr JR, Nunez Y, Kressirer CA, et al. White-spot lesions and gingivitis microbiotas in orthodontic patients. J Dent Res. 2012 Sep;91(9):853–8.
17. Donkor AM, Ahenkorah B, Wallah TA, Yakubu A. Evaluation of extracts from and their herbal ointment for therapeutic and biological activities. Heliyon. 2023 Sep;9(9):e19316.
18. Membe Femoe U, Kadji Fassi JB, Boukeng Jatsa H, Tchoffo YL, Amvame Nna DC, Kamdoum BC, et al. Assessment of the Cercaricidal Activity of Burm. F. and Linn. (Malvaceae) Hydroethanolic Extracts, Cytotoxicity, and Phytochemical Studies. Evid Based Complement Alternat Med. 2022 Jan 10;2022:7281144.
19. Veerakumar K, Govindarajan M, Rajeswary M. Green synthesis of silver nanoparticles using Sida acuta (Malvaceae) leaf extract against Culex quinquefasciatus, Anopheles stephensi, and Aedes aegypti (Diptera: Culicidae). Parasitol Res. 2013 Dec;112(12):4073–85.
20. Jablonski-Momeni A, Korbmacher-Steiner H, Heinzel-Gutenbrunner M, Jablonski B, Jaquet W, Bottenberg P. Randomised in situ clinical trial investigating self-assembling peptide matrix P11-4 in the prevention of artificial caries lesions. Sci Rep. 2019 Jan 22;9(1):269.
21. Justino AB, Teixeira RR, Peixoto LG, Jaramillo OLB, Espindola FS. Effect of saliva collection methods and oral hygiene on salivary biomarkers. Scand J Clin Lab Invest. 2017 Oct;77(6):415–22.
22. Zachrisson BU, Brobakken BO. Clinical comparison of direct versus indirect bonding with different bracket types and adhesives. Am J Orthod. 1978 Jul;74(1):62–78.
23. Manoharan V, Arun Kumar S, Arumugam SB, Anand V, Krishnamoorthy S, Methippara JJ. Is Resin Infiltration a Microinvasive Approach to White Lesions of Calcified Tooth Structures?: A Systemic Review. Int J Clin Pediatr Dent. 2019 Jan-Feb;12(1):53–8.
24. Cai Y, Liao Y, Brandt BW, Wei X, Liu H, Crielaard W, et al. The Fitness Cost of Fluoride Resistance for Different Strains in Biofilms. Front Microbiol. 2017 Aug 28;8:1630.
25. Moraes G, Zambom C, Siqueira WL. Nanoparticles in Dentistry: A Comprehensive Review. Pharmaceuticals [Internet]. 2021 Jul 30;14(8). Available from: http://dx.doi.org/10.3390/ph14080752
26. Kulshrestha S, Khan S, Hasan S, Khan ME, Misba L, Khan AU. Calcium fluoride nanoparticles induced suppression of Streptococcus mutans biofilm: an in vitro and in vivo approach. Appl Microbiol Biotechnol. 2016 Feb;100(4):1901–14.
27. Nguyen S, Escudero C, Sediqi N, Smistad G, Hiorth M. Fluoride loaded polymeric nanoparticles for dental delivery. Eur J Pharm Sci. 2017 Jun 15;104:326–34.
28. Ibrahim MA, Meera Priyadarshini B, Neo J, Fawzy AS. Characterization of Chitosan/TiO Nano-Powder Modified Glass-Ionomer Cement for Restorative Dental Applications. J Esthet Restor Dent. 2017 Apr;29(2):146–56.

29. Covarrubias C, Trepiana D, Corral C. Synthesis of hybrid copper-chitosan nanoparticles with antibacterial activity against cariogenic Streptococcus mutans. Dent Mater J. 2018 Jun 8;37(3):379–84.
30. Sebelemetja M, Moeno S, Patel M. Anti-acidogenic, anti-biofilm and slow release properties of Dodonaea viscosa var. angustifolia flavone stabilized polymeric nanoparticles. Arch Oral Biol. 2020 Jan;109:104586.
31. Liu Y, Busscher HJ, Zhao B, Li Y, Zhang Z, van der Mei HC, et al. Surface-Adaptive, Antimicrobially Loaded, Micellar Nanocarriers with Enhanced Penetration and Killing Efficiency in Staphylococcal Biofilms. ACS Nano. 2016 Apr 26;10(4):4779–89.
32. Singh J, Dutta T, Kim KH, Rawat M, Samddar P, Kumar P. "Green" synthesis of metals and their oxide nanoparticles: applications for environmental remediation. J Nanobiotechnology. 2018 Oct 30;16(1):84.
33. Abolarinwa TO, Ajose DJ, Oluwarinde BO, Fri J, Montso KP, Fayemi OE, et al. Plant-derived nanoparticles as alternative therapy against Diarrheal pathogens in the era of antimicrobial resistance: A review. Front Microbiol. 2022 Dec 15;13:1007115.
34. Saravanan A, Maruthapandi M, Das P, Luong JHT, Gedanken A. Green Synthesis of Multifunctional Carbon Dots with Antibacterial Activities. Nanomaterials (Basel) [Internet]. 2021 Feb 2;11(2). Available from: http://dx.doi.org/10.3390/nano11020369
35. Xiao J, Feng S, Wang X, Long K, Luo Y, Wang Y, et al. Identification of exosome-like nanoparticle-derived microRNAs from 11 edible fruits and vegetables. PeerJ. 2018 Jul 31;6:e5186.
36. Großkopf A, Simm A. Carbohydrates in nutrition: friend or foe? Z Gerontol Geriatr. 2020 Jul;53(4):290–4.
37. Selvaraju N, Ganesh PS, Palrasu V, Venugopal G, Mariappan V. Evaluation of Antimicrobial and Antibiofilm Activity of Fruit Juice Based Carbon Dots against. ACS Omega. 2022 Oct 18;7(41):36227–34.
38. Somboonwiwat K, Marcos M, Tassanakajon A, Klinbunga S, Aumelas A, Romestand B, et al. Recombinant expression and anti-microbial activity of anti-lipopolysaccharide factor (ALF) from the black tiger shrimp Penaeus monodon. Dev Comp Immunol. 2005 Mar 18;29(10):841–51.
39. Liu F, Liu Y, Li F, Dong B, Xiang J. Molecular cloning and expression profile of putative antilipopolysaccharide factor in Chinese shrimp (Fenneropenaeus chinensis). Mar Biotechnol . 2005 Sep 30;7(6):600–8.
40. Kang CJ, Wang JX, Zhao XF, Yang XM, Shao HL, Xiang JH. Molecular cloning and expression analysis of Ch-penaeidin, an antimicrobial peptide from Chinese shrimp, Fenneropenaeus chinensis. Fish Shellfish Immunol. 2004 Apr;16(4):513–25.
41. Supungul P, Klinbunga S, Pichyangkura R, Jitrapakdee S, Hirono I, Aoki T, et al. Identification of immune-related genes in hemocytes of black tiger shrimp (Penaeus monodon). Mar Biotechnol . 2002 Oct;4(5):487–94.
42. Supungul P, Tang S, Maneeruttanarungroj C, Rimphanitchayakit V, Hirono I, Aoki T, et al. Cloning, expression and antimicrobial activity of crustinPm1, a major isoform of crustin, from the black tiger shrimp Penaeus monodon. Dev Comp Immunol. 2008;32(1):61–70.

43. Yang S, Huang H, Wang F, Aweya JJ, Zheng Z, Zhang Y. Prediction and characterization of a novel hemocyanin-derived antimicrobial peptide from shrimp Litopenaeus vannamei. Amino Acids. 2018 Aug;50(8):995–1005.
44. Wang Z, de la Fuente-Núñez C, Shen Y, Haapasalo M, Hancock REW. Treatment of Oral Multispecies Biofilms by an Anti-Biofilm Peptide. PLoS One. 2015 Jul 13;10(7):e0132512.
45. Zhang W, Xu X, Zhang J, Ye T, Zhou Q, Xu Y, et al. Discovery and Characterization of a New Crustin Antimicrobial Peptide from. Pharmaceutics [Internet]. 2022 Feb 14;14(2). Available from: http://dx.doi.org/10.3390/pharmaceutics14020413
46. Zhang J, Li F, Wang Z, Xiang J. Cloning and recombinant expression of a crustin-like gene from Chinese shrimp, Fenneropenaeus chinensis. J Biotechnol. 2007 Jan 20;127(4):605–14.